Journal of Fluids and Structures 18 (2003) 251–267

JOURNAL OF FLUIDS AND STRUCTURES

www.elsevier.nl/locate/jnlabr/yjfls

Excitation and evolution of waves on an inhomogeneous flexible wall in a mean flow

A.D. Lucey[a,*], P.K. Sen[b], P.W. Carpenter[c]

[a] *Department of Mechanical Engineering, Curtin University of Technology, P.O. Box U1987, Perth 6845, Australia*
[b] *Department of Applied Mechanics, I.I.T. Delhi, New Delhi, India*
[c] *Fluid Dynamics Research Centre, University of Warwick, Coventry CV4 7AL, UK*

Received 18 December 2002; accepted 25 July 2003

Abstract

The excitation of neutrally stable small-amplitude waves in a system comprising uniform flow over a flexible wall is studied. Linear theory and numerical simulation are used. A feature of wave excitation in such systems is that distinct amplitude ratios exist when more than one wave is present. An amplitude-ratio equation is first derived for the two waves excited directly by oscillatory excitation applied to a spatially homogeneous plate-spring flexible wall. Thereafter, a second amplitude-ratio equation is derived for waves on a wall with spatially varying foundation-spring stiffness coefficient. In this case, waves beyond a region of changing flexibility are continuously excited by waves propagating through the region of change. Alternatively, it can be considered that an incoming wave evolves into the outgoing wave that emerges from the region of changing wall flexibility. Both energy-flux and WKB methods are used to derive the final amplitude-ratio equation. The theory holds for both upstream- and downstream-propagating waves. It is shown, inter alia, that the waves on either side of the region of slowly changing wall properties are well-described by the dispersion equation based upon local wall properties. Finally, the case of waves incident upon a region of rapidly changing wall properties is simulated and discussed.

1. Introduction

The hydroelastic behaviour of small-amplitude waves has, most often, been studied theoretically using a boundary-value approach with a normal-mode prescription of system waves. Such an approach necessarily assumes a spatially homogeneous system of infinite streamwise extent. It is therefore unable to address the important matter of how disturbances come into being and the subsequent relationship between the excitation that initiates wave motions and the amplitude of the waves that emanate from such forcing. In more recent years, a body of work, for example Crighton and Oswell (1991), Peake (1997), Lucey (1998) and Abrahams and Wickham (2001), has emerged in which the initial-value problem has been solved for the case of oscillatory line excitation in the two-dimensional problem of uniform flow over a thin elastic plate or shell. Such studies show spatial dependence of the response in that particular wave solutions of the dispersion relation are predicted to appear *either* upstream *or* downstream of the point of excitation. The present paper takes up this theme and extends the aforementioned studies by tackling the propagation of waves over a flexible boundary with spatially varying mechanical properties.

The problems addressed in this paper are illustrated by the schematic of Fig. 1. Oscillatory line excitation generates upstream- and downstream-propagating waves of different amplitudes. Our first interest lies in determining the

*Corresponding author. Tel.: +61-8-9266-7047; fax: +61-8-9266-2681.
E-mail address: luceya@vesta.curtin.edu.au (A.D. Lucey).

0889-9746/$ - see front matter © 2003 Elsevier Ltd. All rights reserved.
doi:10.1016/j.jfluidstructs.2003.07.003

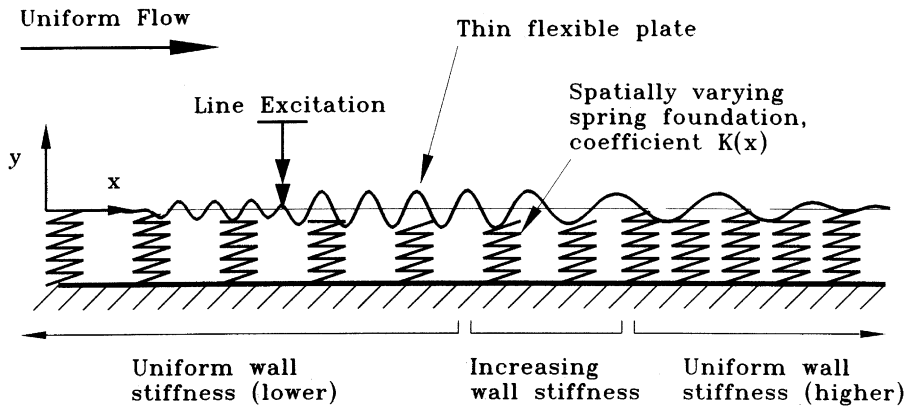

Fig. 1. Schematic of system waves generated by continuous line excitation and subsequent propagation through a region of changing flexible-wall properties.

amplitude ratio of these waves; it is shown that this problem is closely related to the main wave-evolution problem due to a flexible wall with spatially varying properties. After its initial excitation, the downstream wave passes through a region of changing wall flexibility. As it does so it evolves until it emerges with wavenumber and amplitude modified to match the local conditions in the region downstream of the change. An important goal of the present work is to find the amplitude change of the wave in terms of its *local* wave properties upstream and downstream of the region of changing wall stiffness. This problem may also be considered as one of wave excitation in that an output wave with frequency ω, wavenumber k_2 and amplitude η_{02} is generated by an incoming disturbance. In this case, the incoming disturbance is a wave with properties ω, k_1 and η_{01} propagating through an upstream region of different wall flexibility. A subsidiary objective is to confirm that waves in different spatial regions of the overall wall-flow system can be accurately described in terms of the local properties of the system. Although Fig. 1 only depicts the evolution of downstream-propagating waves, we also investigate corresponding phenomena for upstream-propagating disturbances. In this paper we mainly concern ourselves with *slow* variation in the region of wall-property change. However, we briefly consider the limits of our analysis based upon this assumption. Clearly, a combination of wave reflection and transmission can occur if a rapid change in wall properties is prescribed.

In this paper we consider the excitation and propagation of neutrally stable waves. We therefore restrict ourselves to fluid loading at flow speeds lower than those that would yield hydroelastic instability at any spatial location within the system. Moreover, we choose to model the simplest type of spatially varying flexible wall—an elastic plate of invariant properties supported by a spatially varying distributed spring foundation. Our goal, therefore, is to establish a framework of theoretical and computational methods within which more complete flow and wall models can be developed. Although the present problems are of general scientific interest, specific motivation for their study is provided by the potential of compliant coatings to reduce skin-friction drag in marine vehicles. Carpenter et al. (2000, 2001) have proposed that extremely effective laminar-flow control can be achieved by coatings with spatially dependent properties, allowing properties to be tailored to the local Reynolds number. Choi et al. (1997) have experimentally demonstrated that flexible walls can reduce turbulent skin friction. In this application, too, the excitation of fluid-loaded wall waves that might evolve into hydroelastic instability can limit the effectiveness of this drag-reduction strategy. De Langre and Ouvrard (1999) have shown that the open system studied in this paper is closely related to that of plug flow in elastic channels. Clearly, then, further applications for the present work are to be found in biomechanics.

The present paper combines analytical and computational approaches to study the problems illustrated in Fig. 1. Whilst we describe the analytical methods in some detail, the computational method is only briefly summarized because it is a minor development from that formulated and used in Lucey and Carpenter (1992) and Lucey (1998). The simulations that the method permits are, however, an integral part of the present investigation. We therefore divide the remainder of this paper along investigative lines, as opposed to methodologies, in the following way. Section 2 presents the system of equations used to model the system and briefly describes solution methods. In Section 3, we address the problem of wave excitation by an external oscillator. In Section 4, we solve the problem of wave-propagation through a region of spatially varying wall flexibility. Two independent theoretical approaches are developed, one based on energy fluxes, the other at the force level using a WKB method. The predictions of these methods are shown to give good agreement with the results of numerical simulations. Finally, in Section 5, we provide a brief conclusion to the present work.

2. Governing equations

The small-amplitude motion, of a thin elastic plate, supported by a spatially varying spring foundation $K^*(x)$, in the presence of a fluid flow and subjected to oscillatory line excitation is described by

$$\rho_m h\frac{\partial^2\eta}{\partial t^2}+B\frac{\partial^4\eta}{\partial x^4}+K^*(x)\eta=-p(x,0,t)+F_0^*\exp(\mathrm{i}\omega_F t)\delta(x-x_F)\mathrm{H}(t), \tag{1}$$

where $\eta(x,t)$, ρ_m, h and B are, respectively, plate's deflection, density, thickness and flexural rigidity, while $p(x,y,t)$ is the unsteady fluid pressure and F_0^*, ω_F and x_F are, respectively, the amplitude, frequency and location of the line excitation. H and δ are the Heaviside and delta functions.

Assuming the flow to be incompressible and irrotational, a velocity perturbation potential $\phi(x,y,t)$ which satisfies Laplace's equation,

$$\nabla^2\phi=0, \tag{2}$$

can be introduced along with the condition $\phi\to 0$ as $y\to\infty$ that enforces disturbance decay with vertical distance from the fluid–wall interface. The unsteady fluid pressure can be found from the linearized Bernoulli relation

$$p=-\rho_f\frac{\partial\phi}{\partial t}-\rho_f U^*\frac{\partial\phi}{\partial x}, \tag{3}$$

where ρ_f and U^* are, respectively, the fluid density and flow speed. The plate and fluid motions are coupled through the kinematic boundary condition

$$\frac{\partial\phi}{\partial y}=\frac{\partial\eta}{\partial t}+U^*\frac{\partial\eta}{\partial x}, \tag{4}$$

which, in the linearized system, is enforced at $y=0$.

The system of equations is then nondimensionalized using a reference lengthscale, l_{ref} and timescale t_{ref} defined by

$$l_{\mathrm{ref}}=\frac{\rho_m h}{\rho_f}\quad\text{and}\quad t_{\mathrm{ref}}=\frac{(\rho_m h)^{5/2}}{\rho_f^2 B^{1/2}}. \tag{5a, b}$$

In doing so we follow the convention used by Brazier-Smith and Scott (1984) and Crighton and Oswell (1991) the choice of which reduced their equivalent (unsupported) elastic-plate problem to a system of equations with just one nondimensional control parameter, namely the flow speed.

The equations for the resulting nondimensional variables are identical to Eqs. (1)–(4) with $(\rho_m h)=B=\rho_f=1$ and having replaced the system parameters with their nondimensional counterparts

$$U=\frac{t_{\mathrm{ref}}}{l_{\mathrm{ref}}}U^*,\quad K=\frac{l_{\mathrm{ref}}^4}{B}K^*,\quad F_0=\frac{l_{\mathrm{ref}}^3}{B}F_0^*. \tag{6}$$

Only U and K are control parameters for the dynamics of the system. The value of F_0 simply determines the amplitude of perturbations in the system. We also note that the nondimensional perturbation pressure and potential are, respectively, $p\,l_{\mathrm{ref}}^3/B$ and $\phi/(l_{\mathrm{ref}}t_{\mathrm{ref}})$.

For a spatially homogeneous system ($K(x)=K_0$) of infinite extent and without line excitation ($F_0=0$), the nondimensional equations are readily solved—for example, see Carpenter and Garrad (1986)—by assuming all disturbances to be proportional to the travelling-wave form $\exp[\mathrm{i}(kx-\omega t)]$. This gives

$$\eta(x,t)=\eta_0\exp[\mathrm{i}(kx-\omega t)], \tag{7a}$$

$$\phi(x,y,t)=\frac{\mathrm{i}}{|k|}(\omega-Uk)\exp(-|k|y)\eta, \tag{7b}$$

$$p(x,y,t)=-\frac{1}{|k|}(\omega-Uk)^2\exp(-|k|y)\,\eta, \tag{7c}$$

where k and ω satisfy the dispersion equation

$$D(k,\omega)=\omega^2-k^4+\frac{(\omega-Uk)^2}{|k|}-K=0. \tag{8}$$

These results will be invoked in the following sections as wave solutions corresponding to *local* properties in a spatially inhomogeneous wall–flow system. However, we remain aware that they are strictly appropriate to a spatially infinite

domain of such local properties. Finally, Lucey and Peake (2003) have shown that the system can support unstable waves if $U > U_D$ where U_D, the static-divergence onset speed, is given by

$$U_D = 2(3)^{-3/8}K^{3/8}. \tag{9}$$

The work in this paper is restricted to phenomena of the flow-speed range $U < U_D$ in which neutrally stable waves comprise the system response.

Fig. 2 shows a plot of the dispersion equation for $U = 0.02487$ and two values of the coefficient of foundation-spring stiffness, K. Positive(negative) values of the wavenumber, k, correspond to waves with downstream(upstream) directed phase velocity. Because we restrict our attention to the flow-speed range $U < U_D$, the system only supports conventional flexural waves modified by fluid loading. These are positive positive-energy waves (or Class B waves in the Benjamin–Landahl classification scheme). These waves then correspond to the k_3^- and k_2^+ types of wave found, respectively, upstream and downstream of the driver in the Crighton and Oswell (1991) problem. For these waves, Crighton and Oswell show that the group velocity, $c_g = \partial\omega/\partial k$ correctly predicts the speed and direction of wave-energy flux. It is evident from Fig. 2 that the direction of the group velocity and phase velocity, ω/k are the same for the class of waves studied herein. Thus, solutions with +ve(−ve) k would appear downstream(upstream) of a source of initial or continuous excitation, for example the oscillatory line exciter depicted in Fig. 1. The discrete data marked in Fig. 2 represent waves found in the numerical simulations presented in subsequent figures and will be discussed later in the paper.

The numerical simulations presented in this paper are generated by a computational approach that combines boundary-element and finite-difference methods to solve the governing equations. Singularities satisfying the Laplace equation (2), are spread over the wall–flow interface, their intensities being determined by the kinematic boundary condition, Eq. (4). The pressure is then evaluated using Eq. (3) at discrete interfacial points. The pressure, along with the line forcing, is used to drive the left-hand side of Eq. (1) written in finite-difference form. Lucey and Carpenter (1992) and Lucey (1998) provide details of the method. Such computations require the flexible wall to be of finite length, L. The boundary conditions on plate motion at $x = 0, L$ model a plate with hinged ends. To mimic an infinitely long wall, we choose L to be large relative to disturbance wavelength. We also introduce some highly localized structural damping that is only significant in the vicinity of $x = 0, L$. This is equivalent to including an additional term of the form $d(x)\partial\eta/\partial t$ on the left-hand side of Eq. (1), where the damping coefficient, $d(x)$, is effectively zero everywhere except in the immediate vicinity of $x = 0, L$. This serves to eliminate reflection of the neutrally stable waves at the wall's fixed ends thereby giving a system that best approximates the undamped flexible wall of infinite extent that is addressed by the

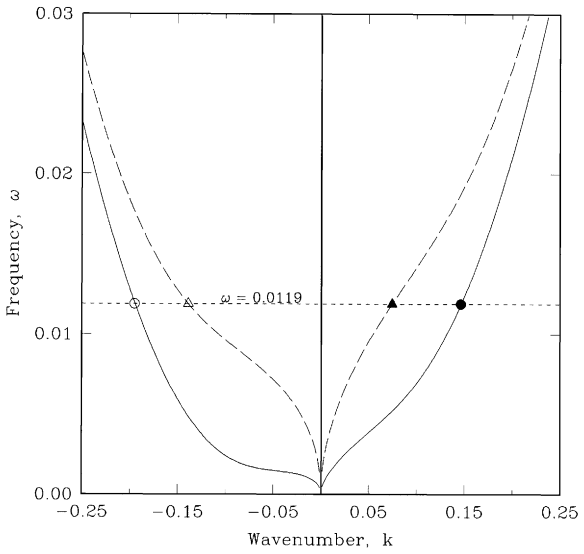

Fig. 2. Dispersion diagram, at $U = 0.02487$, for the plate-spring flexible wall for two values of spring-foundation stiffness, low, $K = 0.1463 \times 10^{-3}$, (——) and high, $K = 1.463 \times 10^{-3}$, (- - -). The frequency marked ($\omega = 0.0119$) is that of waves excited in the numerical simulations presented in this paper with discrete data points locating waves found: upstream (◦), and downstream (•), of exciter in Fig. 3a; upstream (◦) of exciter and downstream of exciter before (•), and after (▲), region of changing wall properties in Fig. 5; and downstream (•) of exciter and upstream of exciter before (◦), and after (△), region of changing wall properties in Fig. 7.

theoretical modelling. Clearly, there remain important differences between the finite system of the simulations and the one analysed theoretically. We therefore note that, in this paper, the use of terms applied to describe the direction of disturbance properties is not mathematically exact for a flexible wall of finite length. By necessity, we apply engineering usage to directional descriptions; these characterize the behaviour of disturbances on the basis of the dominant element of their wave content.

3. Line excitation: wave–amplitude ratios

In this section we consider a spatially homogeneous flexible wall with line excitation at a frequency ω_F. Typical simulations for two flow speeds, $U = 0.02487$ and 0.0496, are shown in Fig. 3 for excitation with $\omega_F = 0.0119$ and amplitude $F_0 = 30.03 \times 10^{-6}$. The spring-stiffness coefficient, K, is 0.1463×10^{-3}. Eq. (9) gives $U_D = 0.0483$ and thus our higher flow speed is marginally in excess of the theoretical divergence-onset critical flow speed based upon a wall of infinite length. In our finite system, the restraints at the ends of the flexible wall effectively increase the wall's restorative stiffness, thereby giving a slightly higher critical flow speed. The length of the wall is $738 l_{\mathrm{ref}}$ and the instantaneous wall profiles in the figures occur at $2680 t_{\mathrm{ref}}$ after starting up the excitation, the system having reached a steady dynamic state. Most transients excited in the start-up procedure have died away and the continuous power input of the exciter is concurrently extracted by the structural damping close to the flexible-wall ends. Upstream- and downstream-propagating waves continuously emanate from the driver. Upstream, the wave has properties k_U and η_{0U} whereas the downstream wave has k_D and η_{0D}; both have $\omega = \omega_F$. These waves are found to be solutions to the dispersion equation (8). The frequency–wavenumber values of the upstream- and downstream-propagating waves on either side of the line excitation in Fig. 3a are marked in Fig. 2. The significant feature of Fig. 3 is the amplitude difference between the upstream and downstream waves. These, and other, simulations show that the amplitude ratio, $A_{DU} = \eta_{0D}/\eta_{0U}$, is dependent on U and ω_F and this dependence is summarized in Fig. 4.

We now seek to derive an analytical prediction for the amplitude ratios that can be deduced from Fig. 3. We follow the methods of Brazier-Smith and Scott (1984) and Crighton and Oswell (1991). To find the long-time response we take Fourier transforms in both space and time of Eqs. (1)–(4). The resulting set of linear algebraic equations are then solved to find the deflection transform. The actual deflection is then obtained by evaluating the inverse transforms to give

$$\eta(x,t) = \frac{F_0}{2\pi}\,\Psi(\omega_F, x)\exp(-\mathrm{i}\omega_F t), \tag{10a}$$

where

$$\Psi(x,\omega) = \int_{-\infty}^{\infty} \frac{\exp(-\mathrm{i}kx)}{D(k,\omega)}\,\mathrm{d}k, \tag{10b}$$

and $D(k,\omega)$ is defined in Eq. (8). To extract the poles, k_i, that contribute to Ψ, we factorize D using a first-order Taylor expansion about the required wavenumber; thus $D = (k - k_i)D_{,k}(k_i,\omega)$ because $D(k_i,\omega) = 0$. In completing the

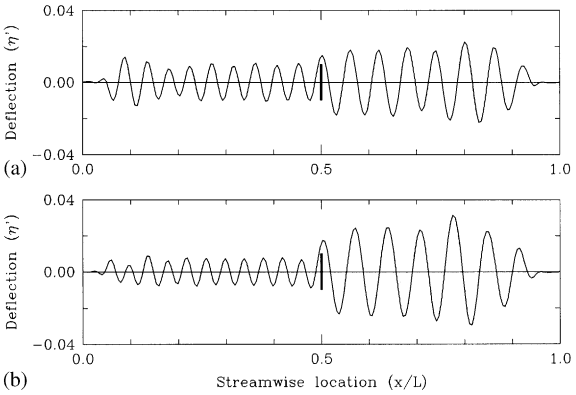

Fig. 3. Typical instantaneous wall profiles for a homogeneous flexible panel with $K = 0.1463 \times 10^{-3}$ undergoing continuous oscillatory line excitation at frequency $\omega_F = 0.0119$ (position denoted by a thick vertical line) in a uniform flow from left to right at (a) $U = 0.02487$, and (b) $U = 0.0496$. (Here, and in Figs. 5c, 7c and 9c, the deflection has been non-dimensionalized with respect to plate thickness; for the data used throughout this means that $\eta' = 2.71\eta$.)

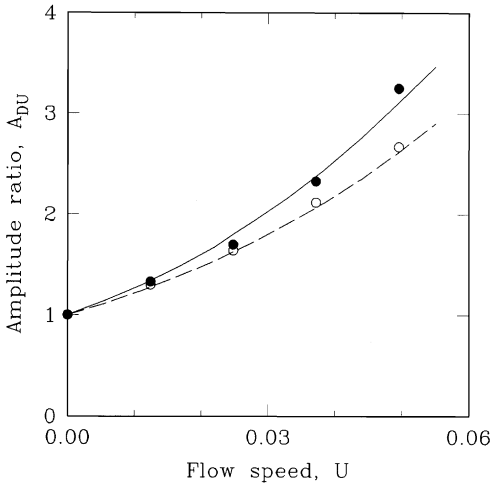

Fig. 4. Wave–amplitude ratio versus flow speed for the pair of waves that emanate from continuous oscillatory excitation for $K = 0.1463 \times 10^{-3}$ and two frequencies, $\omega_F = 0.0119$ (—— and •) and $\omega_F = 0.0159$ (– – – and ◦); continuous data from Eqs. (12), discrete data are results from numerical simulations.

integration of Eq. (10b) the causality condition determines the validity of contributing poles associated with k_U and k_D associated with the far-field solutions upstream and downstream, respectively, of the line excitation at $x = x_F$. This process yields

$$\Psi(x,\omega_F) = \begin{cases} \dfrac{2\pi i k_U^2 \exp(ik_U x)}{4k_U^5 + (|k_U|/k_U)(\omega_F^2 - U^2 k_U^2)} & \text{for } x < x_F, \\ \dfrac{2\pi i k_D^2 \exp(ik_D x)}{4k_D^5 + (|k_D|/k_D)(\omega_F^2 - U^2 k_D^2)} & \text{for } x > x_F. \end{cases} \tag{11}$$

Clearly, the waves upstream and downstream of the exciter obtained when Eq. (11) is used in Eq. (10a) are alone insufficient to complete the near-field solution. At $x = x_F$ further conditions apply. These require continuity of deflection, slope, curvature and a shear-force discontinuity, equalling the applied excitation, between the upstream and downstream solutions. In each of the upstream and downstream regions $D(k,\omega) = 0$ has one real and two pairs of complex conjugate solutions. The far-field solutions, k_U and k_D, are the real solutions displayed in Fig. 2. For the near-field solutions, the evanescent modes, given by the spatially decaying complex solutions of $D(k,\omega) = 0$ contribute to the complete solution so that the conditions at $x = x_F$ are satisfied. This type of wave superposition is conducted in Davies and Carpenter (1997) who constructed the full solution for the near-field of a rigid-compliant join for boundary-layer flow over a finite compliant panel. In the present paper, we only concern ourselves with the far-field solutions that strictly apply in the asymptotic limit $x \to \pm\infty$. However, in practice close inspection of our numerical results in the vicinity of $x = x_F$ shows that the evanescent-mode components of the response are negligible beyond approximately one disturbance (far-field) wavelength from the exciter.

We can now consider the amplitude ratio of the far-field waves in the regions upstream and downstream of the exciter. The use of solutions (11) in conjunction with Eq. (10a) leads to the amplitude ratio A_{DU} $(= \eta_{0D}/\eta_{0U})$ being given by

$$A_{DU} = \left| \frac{4k_U^3 + (\omega_F^2 - U^2 k_U^2)/(|k_U|k_U)}{4k_D^3 + (\omega_F^2 - U^2 k_D^2)/(|k_D|k_D)} \right| \tag{12a}$$

with

$$D(k_U,\omega_F) = 0 \quad \text{and} \quad D(k_D,\omega_F) = 0. \tag{12b, c}$$

The variation of A_{DU} with U is plotted, for two values of ω_F in Fig. 4. Clearly, there is good agreement between the result of Eqs. (12) and the results of our numerical simulations.

The absence of K-dependence in Eq. (12a) indicates that the energy input by the exciter divides itself between the upstream and downstream waves on the basis of wave energy-density propagation. This is because the mechanics of the spring-foundation play no part in energy-density propagation, there being no coupling of the $K\eta$ term in Eq. (1) with

adjacent spatial locations. However, in this section, we do not attempt to formulate an energy-flux balance because Crighton and Oswell (1991) have shown that only approximate expressions can be obtained for the rate at which the exciter imparts energy to the flexible wall.

We also find that the algebraic expression common to the numerator and denominator in Eq. (12a), respectively, yields negative and positive values for the solutions to Eqs. (12b) and (12c). This is because the solutions, respectively, give −ve values +ve values for k_U and k_D in the flow-speed range of neutrally stable waves, as seen in Fig. 2. Thus, the sign of the evaluated algebraic expression that appears in both numerator and denominator of Eq. (12a) is an indicator of the direction of wave energy-density propagation. In closing this section, we remark that this expression will be shown below to quantify a wave property that also characterizes the evolution of waves propagating over changing flexible-wall properties.

4. Wave propagation through a change in wall properties

We now study the passage of a disturbance, commencing as a wave with frequency ω, wavenumber $k_1 = k(x_1)$ and amplitude $\eta_{01} = \eta_0(x_1)$ in region 1, through a region of prescribed change in wall flexibility. It ultimately propagates through region 2 which has uniform wall flexibility (different to that of region 1) as a wave with properties ω, $k_2 = k(x_2)$ and $\eta_{02} = \eta(x_2)$. In the region of changing wall properties ($x_1 < x < x_2$, for a downstream-propagating disturbance) both $k(x)$ and $\eta_0(x)$ have continuous variation with the streamwise coordinate. A typical numerical simulation of this phenomenon is summarized in Fig. 5. With the exception of K, the physical data are identical to those used to generate Fig. 3a. For the spatially inhomogeneous flexible wall K has been chosen to vary as the reciprocal error function,

$$K(x') = K_2 - \frac{1}{2}(K_2 - K_1)\left[1 - \mathrm{erf}\left(\frac{x' - x'_0}{\sigma}\right)\right], \tag{13}$$

where $x' = x/L$ and L is the dimensional length of the entire flexible panel. In Eq. (13), K_1 and K_2 are, respectively, the values of K upstream and downstream of the change which is centred on x'_0 and has a variance, σ. For Fig. 5, we choose $x'_0 = 0.5$, $\sigma = 0.1$ and $K_2/K_1 = 10$ where $K_1 = 0.1463 \times 10^{-3}$. The resulting variation of the coefficient of foundation-spring stiffness has been plotted in Fig. 5b. We note that the change principally occurs in the region x': $0.4 \rightarrow 0.6$. Region 1 of the flexible wall lies upstream, whilst region 2 is downstream, of the change.

Fig. 5a shows the evolution of waves in the system in space–time form. Oscillatory line excitation at $x' = 0.2$ with $\omega_F = 0.0119$ continuously excites a downstream-propagating wave in region 1 which we take to lie approximately in the range x': $0.2 \rightarrow 0.35$. Concurrently, an upstream-propagating wave is generated in the region x': $0 \rightarrow 0.2$. This wave is damped out by the high structural damping in the region close to the leading edge of the flexible wall and it will no longer concern us in what follows. As time passes, the leading edge of the downstream-propagating wave enters the region of decreasing wall flexibility adapting as it does so until emerges into region 2 approximately defined by x': $0.65 \rightarrow 1$. The wave that has developed in region 2 can be seen to have both lower wavenumber and amplitude than the upstream wave in region 1 which excited it. This contrast is brought out in Fig. 5c in which the last instantaneous wall profile of Fig. 5a has been plotted along with the corresponding result for a homogeneous flexible wall with $K = K_1$.[1] The coincidence of the two profiles upstream of $x' = 0.35$ confirms that no waves are reflected from the region of wall-property variation. Moreover, it suggests that the wave in region 1 is not influenced by downstream phenomena and that its characteristics can be captured by the *local* properties of the wall–flow system. Measurements of the waves seen in Figs. 5a and 5c find that $\omega_1 = \omega_2 = \omega_F$ and that both $D_1(k_1, \omega) = 0$ and $D_2(k_2, \omega) = 0$ where D_1 and D_2 are, respectively, the dispersion relation of Eq. (8), with $K = K_1$ and K_2. Note that we have dropped the suffices on ω because the angular frequency is found to be the same in both regions. The frequency–wavenumber properties of the waves before and after the region of changing wall properties have been marked in Fig. 2. These findings are reproduced in other simulations for which the change in wall properties is slow. They suggest that waves upstream and downstream of a region of change can be characterized by the dispersion equation applied locally despite the fact that it is strictly applicable only to a homogeneous wall of infinite streamwise extent. Of course, the dispersion model cannot say anything about the amplitude change that occurs between regions 1 and 2. Theoretical means to predict the amplitude change are therefore developed below.

[1] Fig. 5c also shows that the (k_1, ω_1)-wave has a higher group velocity than its successor, the (k_2, ω_2)-wave. On the homogeneous flexible wall, the former has convected to occupy all of x': $0.2 \rightarrow 1$ whereas the latter has not reached the trailing edge of the inhomogeneous flexible wall in the same time period. The difference in group velocity can be predicted by contrasting the value of $\partial D(k, \omega)/\partial k$ for the two waves using Fig. 2.

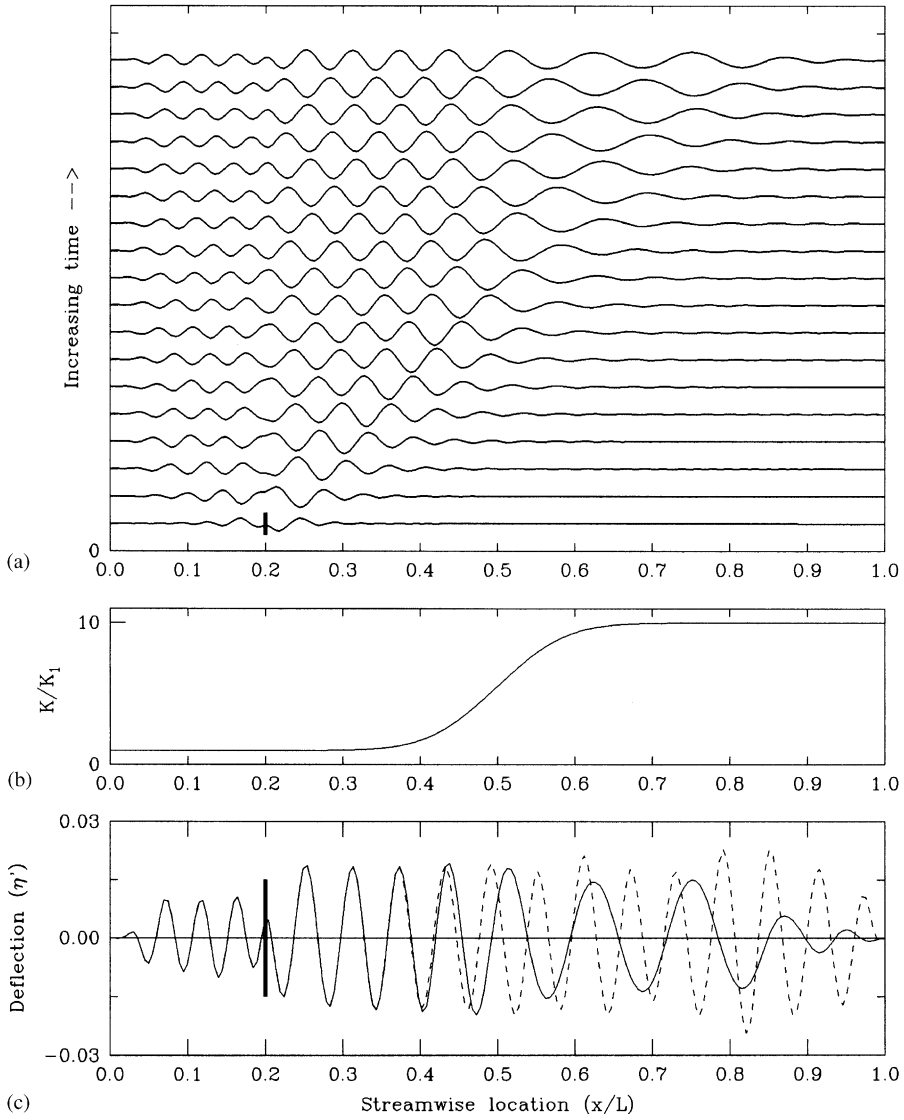

Fig. 5. Propagation of waves from applied oscillatory excitation at $x'_F = 0.2$ (thick vertical line) with frequency $\omega_F = 0.0119$ on a spatially inhomogeneous flexible wall for $U = 0.02487$: (a) wall profiles in space–time form (first profile at $268t_{\text{ref}}$ after excitation start-up and subsequent profiles separated by $268t_{\text{ref}}$), (b) Variation of spring-stiffness coefficient along wall, where $K_1 = 0.1463 \times 10^{-3}$, $x'_0 = 0.5$ and $\sigma = 0.1$, and (c) comparison of waves for a homogeneous, $K/K_1 = 1$, wall (– – –) and those on the spatially varying flexible wall (——) at $4824t_{\text{ref}}$ after start-up.

4.1. Amplitude prediction: energy-flux approach

Given the wave properties in regions 1 and 2, we seek to determine the amplitude ratio, $A_{21} = \eta_{02}/\eta_{01}$ for the waves transmitted from region 1 to region 2. The absence of dissipation, either through structural damping or fluid viscosity, in the region of changing wall properties, permits our goal to be achieved by an energy-flux balance. To do this, we apply the analysis developed by Crighton and Oswell (1991) for a fluid-structure energy balance that includes a source term, namely the line exciter. In our analysis there is no external source term within the control volume under consideration and so our concern is with the fluxes in a spatially inhomogeneous system. We establish a control volume for the fluid that is demarcated by the interface from x_1 in region 1 to x_2 in region 2 and from $y = \eta \to \infty$ at each of $x = x_1$ and $x = x_2$. The control volume is closed between x_1 and x_2 at $y = \infty$ although we do not need to consider fluxes across this boundary because all fluid perturbations decay as $\exp(-|k|y)$ as seen in Eqs. (7b) and (7c). The

flexible-wall energy equation is simply formulated for the one-dimensional space between x_1 and x_2. Clearly, wall and fluid energy balances are coupled and must be combined to give the system energy equation.

The wall energy equation is obtained by omitting the line-excitation term in the nondimensional version of Eq. (1) (since $x_F \notin [x_1, x_2]$), multiplying the equation by $\partial\eta/\partial t$ and integrating from x_1 to x_2. After integration by parts of the flexure term, we have

$$\underbrace{\frac{\mathrm{d}}{\mathrm{d}t}\left\{\frac{1}{2}\int_{x_1}^{x_2}\left[\left(\frac{\partial\eta}{\partial t}\right)^2+\left(\frac{\partial^2\eta}{\partial x^2}\right)^2+K(x)\eta^2\right]\mathrm{d}x\right\}}_{T_P+V_P+V_K}+\underbrace{\left[\frac{\partial^3\eta}{\partial x^3}\frac{\partial\eta}{\partial t}-\frac{\partial^2\eta}{\partial x^2}\frac{\partial^2\eta}{\partial t\partial x}\right]_{x_1}^{x_2}}_{J_P}$$
$$=-\int_{x_1}^{x_2}p_w\frac{\partial\eta}{\partial t}\mathrm{d}x, \tag{14}$$

where $p_w = p(x, 0, t)$. The left-hand side is clearly the temporal rate of change of wall energy, comprising kinetic T_P, plate-bending energy V_P and stored spring energy V_K, *within* the control region plus the net flux out of it, J_P. The symbols used for these terms follow the notation introduced by Crighton and Oswell (1991). The right-hand side is effectively a source term that transfers fluid energy into, or out of, the flexible wall.

Attention is now turned to the fluid-energy equation, the objective being to obtain a term identical to the right-hand side of Eq. (14) that couples the wall and fluid energy equations. The Euler equation for the total fluid velocity, $(U+u)\mathbf{i}+v\mathbf{j}$ (where $\nabla\phi = u\mathbf{i}+v\mathbf{j}$), is first linearized and the dot product with $\nabla\phi$ is then taken to give

$$\frac{\partial\frac{1}{2}(\nabla\phi)^2}{\partial t}+\nabla\cdot[(p+Uu)\nabla\phi]=0. \tag{15}$$

Integrating over the control volume and using the divergence theorem then gives

$$\frac{\mathrm{d}}{\mathrm{d}t}\left\{\int_0^\infty\int_{x_1}^{x_2}\frac{1}{2}(\nabla\phi)^2\,\mathrm{d}x\,\mathrm{d}y\right\}+\underbrace{\left[\int_0^\infty(p+Uu)u\,\mathrm{d}y\right]_{x_1}^{x_2}}_{J_F}$$
$$-\int_{x_1}^{x_2}(p+Uu)v\,\mathrm{d}x\Big|_{y=0}=0. \tag{16}$$

The term J_F is clearly a net fluid-energy flux term. The third term effectively represents energy-transfer between the flexible wall and fluid flow because nonzero v at the interface only occurs when there is wall motion. It is from this term that the integral on the right-hand side of equation (14) can be developed. The first term clearly represents a measure of the rate of change of a fluid energy *within* the control volume. Crighton and Oswell (1991) were careful to note that it is not the variation of *perturbation* kinetic energy. However, the integral is related to the perturbation kinetic energy, T_F, because

$$T_F=\int_\eta^\infty\int_{x_1}^{x_2}\frac{1}{2}((U+u)^2+v^2-U^2)\mathrm{d}x\,\mathrm{d}y$$
$$=\int_0^\infty\int_{x_1}^{x_2}\frac{1}{2}(\nabla\phi)^2\,\mathrm{d}x\,\mathrm{d}y-\int_{x_1}^{x_2}U\eta u\,\mathrm{d}x\Big|_{y=0}+\mathcal{O}(\eta^2). \tag{17}$$

Returning to the third term in Eq. (16), it can be shown, after some manipulation using the nondimensional forms of Eqs. (3) and (4), that it is equal to

$$U\int_{x_1}^{x_2}\left(\frac{\partial\phi}{\partial x}\frac{\partial\eta}{\partial t}-\frac{\partial\phi}{\partial t}\frac{\partial\eta}{\partial x}\right)_{y=0}\mathrm{d}x+\int_{x_1}^{x_2}p_w\frac{\partial\eta}{\partial t}\mathrm{d}x. \tag{18}$$

This expression and Eq. (17), are then used to rewrite the fluid energy equation, (16), as

$$\frac{\mathrm{d}T_F}{\mathrm{d}t}+J_F+\underbrace{\left[U\eta\frac{\partial\phi}{\partial t}\right]_{x_1}^{x_2}}_{J_{PF}}=\int_{x_1}^{x_2}p_w\frac{\partial\eta}{\partial t}\mathrm{d}x. \tag{19}$$

The term J_{PF} represents the net transport, by the nonzero mean flow, of energy associated with the displacement of fluid mass that adds to the wall mass during motion.

The flexible-wall and fluid energy equations, (14) and (19), can now be added to yield the system energy equation

$$\frac{\mathrm{d}}{\mathrm{d}t}(T_F + T_P + V_P + V_K) = \left[\frac{\partial^3\eta}{\partial x^3}\frac{\partial\eta}{\partial t} - \frac{\partial^2\eta}{\partial x^2}\frac{\partial^2\eta}{\partial t\partial x}\right]_{x_2}^{x_1} + \left[\int_0^\infty (p + Uu)u\,\mathrm{d}y\right]_{x_2}^{x_1} + \left[U\eta\frac{\partial\phi}{\partial t}\right]_{x_2}^{x_1}, \tag{20}$$

which takes exactly the same form as the energy equation derived by Crighton and Oswell (1991). Here, we note the presence of stored spring energy on the left-hand side. Again, we emphasize that the distributed spring foundation does not contribute to energy flux in the x-direction because it does not provide spatial coupling of the wall mechanics.

We now evaluate Eq. (20) for the problem at hand. All of our simulations indicate that, after a disturbance has become established in the region $[x_1, x_2]$, it achieves a fluctuating state that is time independent in terms of amplitude, frequency and wavenumber; for example, see the state represented by the last five profiles in Fig. 5a. We therefore hypothesize that a steady state has been reached that makes the left-hand side of Eq. (20) zero. We now balance the flux terms on either side of the region of change in flexible-wall properties. Eqs. (7) are used in the flux terms and integration is carried out over one cycle of oscillation; in doing so it is sufficient simply to consider the real part of each of η, ϕ, u and p because we are exclusively studying neutrally stable waves. Rearrangement then leads to an equation for the ratio of the amplitude of the wave leaving, to that of the wave entering, the region of changing wall properties,

$$A_{21} = \frac{\eta_{02}}{\eta_{01}} = \left[\frac{4k_1^3 + (\omega^2 - U^2k_1^2)/(|k_1|k_1)}{4k_2^3 + (\omega^2 - U^2k_2^2)/(|k_2|k_2)}\right]^{1/2}, \tag{21a}$$

with

$$D_1(k_1, \omega) = 0 \quad \text{and} \quad D_2(k_2, \omega) = 0. \tag{21b, c}$$

The variation with flow speed of the amplitude ratio for downstream-propagating waves is plotted in Fig. 6 for two values of K_2/K_1; as before, we have chosen $K_1 = 0.1463 \times 10^{-3}$. Clearly, A_{21} is a function of U, ω, K_1 and K_2. Although we have solely considered a region in which the flexible-wall stiffness *increases*, the result of Eqs. (21) is equally applicable to a flexible wall with a prescribed *decrease* in wall stiffness. In Fig. 6 we also include data points obtained from a number of numerical simulations similar to that which generated Fig. 5. Good agreement is found between the

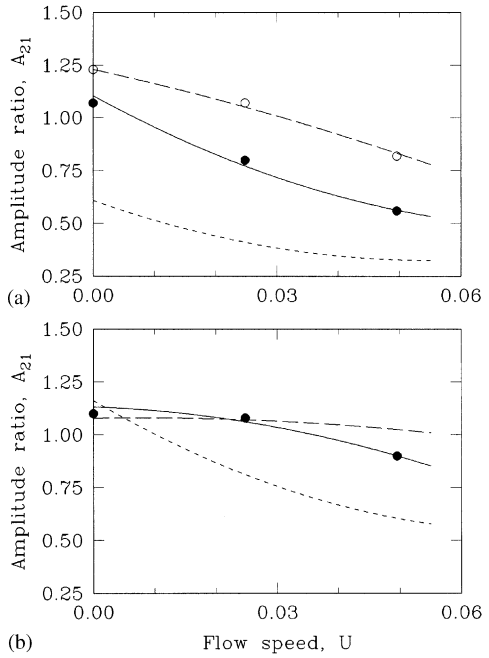

Fig. 6. Wave-amplitude ratio versus flow speed for downstream-propagating waves passing through a region of increasing wall stiffness for three frequencies, $\omega_F = 0.0159$ (– – – and ◦), $\omega_F = 0.0119$ (—— and •) and $\omega_F = 0.0079$ (- - - - -); continuous data from equations (21) discrete data are results from numerical simulations. $K_1 = 0.1463 \times 10^{-3}$ with in (a) $K_2/K_1 = 10$ and (b) $K_2/K_1 = 4$.

theoretical predictions and the results of simulations. For a definitive validation of the result of Eq. (21) we will show below, in Section 4.2, that it can be derived through a completely different approach.

The theoretical analysis developed above also applies to neutrally stable waves propagating in the upstream direction over a region of changing wall properties. Results of a typical numerical simulation of this situation are given in Fig. 7, the layout of which is identical to Fig. 5. All fluid, flexible-wall and exciter parameters are identical to those that generated Fig. 5 except that the oscillatory line excitation is applied at $x' = 0.8$. Our interest here lies in the evolution of the wave in the region upstream of the line-excitation. For this case properties of the incoming and outgoing wave

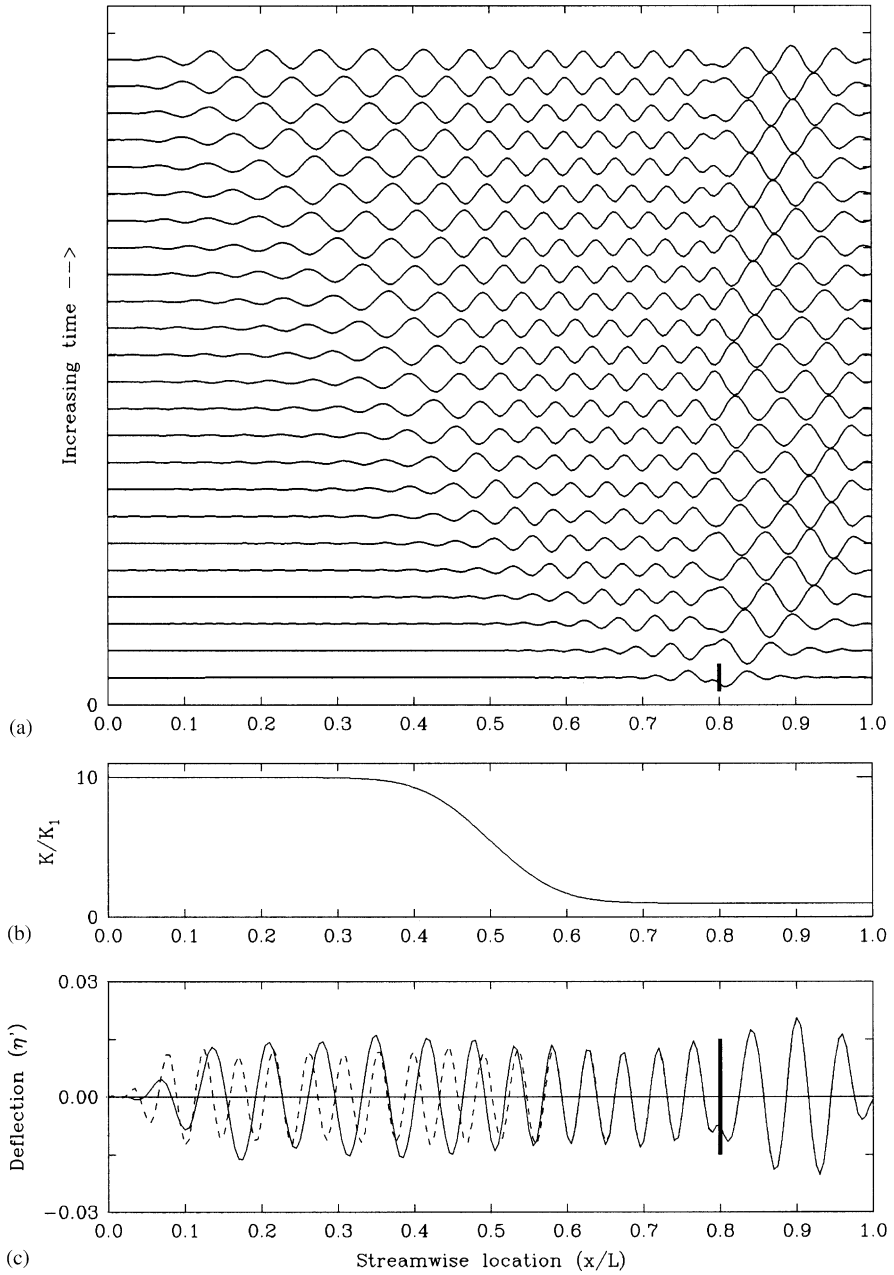

Fig. 7. Propagation of waves from applied oscillatory excitation at $x_F/L = 0.8$ (thick vertical line) through an upstream region of varying flexible-wall properties: (a) Wall profiles in space–time form, (b) Variation of spring-stiffness coefficient along wall, and (c) Comparison of waves for a homogeneous, $K/K_1 = 1$, wall (– – –) and those on the spatially varying flexible wall (——) at $6432t_{\text{ref}}$ after start-up. All other data are identical to those of Fig. 5.

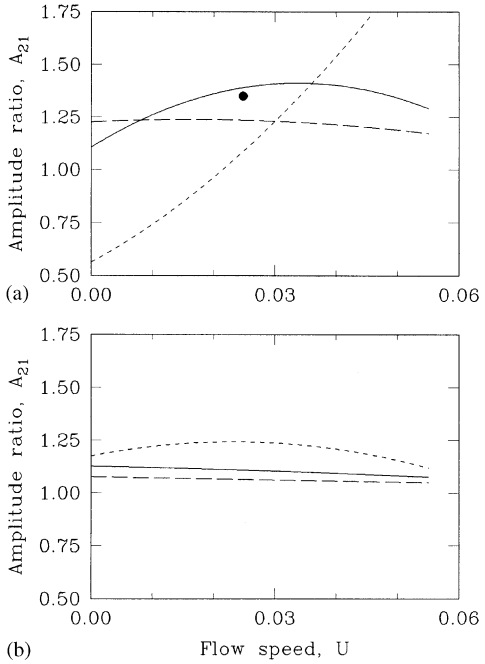

Fig. 8. Wave–amplitude ratio versus flow speed for upstream-propagating waves passing through a region of increasing wall stiffness for three frequencies, $\omega_F = 0.0159$ (– – –), $\omega_F = 0.0119$ (—— and • for the result of Fig. 7) and $\omega_F = 0.0079$ (- - - - -); continuous data from equations (21). $K_1 = 0.1463 \times 10^{-3}$ with in (a) $K_2/K_1 = 10$ and (b) $K_1/K_2 = 4$.

continue to carry the suffices $()_1$ and $()_2$ but it should now be noted that x_1 lies in the region downstream, and x_2 upstream, of the region of changing wall flexibility. The frequency–wavenumber properties of the incoming and outgoing waves are marked in Fig. 2. Again, the dispersion relation based on local wall properties provides an excellent description of the waves on either side of the region of changing wall properties. Figs. 7a and c show that the amplitude of the outgoing wave is greater than that of the incoming wave and the corresponding amplitude ratio is predicted by Eqs. (21). When evaluating Eq. (12a) it is now found that the expressions in the numerator and denominator both yield negative quantities because both incoming and outgoing waves are upstream propagating with negative wavenumbers. Finally, we summarize the amplitude-ratio predictions for upstream-propagating waves in Fig. 8. It should be recalled here, and in Fig. 6, that the theoretical predictions are strictly only valid for $0 \leqslant U < U_D$, where $U_D = 0.0485$ based on the lowest value of K in the system. Like Fig. 6, its counterpart for downstream-propagating waves, we note that a disturbance amplitude may either decrease or increase as it evolves through a region of changing wall-properties. Such amplitude changes are dependent on the combination of flow speed, wave frequency and the mechanical properties of the wall on either side of the region of change.

4.2. Amplitude prediction: the WKB approach

The amplitude-ratio result of Section 4.1 was derived through the principle of energy conservation. In contrast, we now analyse the fluid–structure system 'at the force level'. As before, our goal is to relate the amplitudes of neutrally stable waves on either side of a region of changing flexible-wall properties. It is assumed that the precursor wave in region 1 has wavenumber, k_1 and frequency ω satisfying the local dispersion equation (21b) and the emergent wave has k_2 and ω satisfying Eq. (21c). As reported above, our simulations demonstrate that these assumptions are realistic.

For convenience, we write the equation for wall motion, in the absence of line excitation, as

$$[L_w]\eta = -p_w, \tag{22}$$

the differential operator $[L_w]$ being readily deduced from the nondimensional form of the left-hand side of Eq. (1). Further, we introduce the (nondimensional) linearized equation for y-momentum of the fluid,

$$\frac{\partial v}{\partial t} + U\frac{\partial v}{\partial x} = -\frac{\partial p}{\partial y}, \tag{23}$$

and combine this with the nondimensional form of the kinematic boundary condition (4) to give

$$[L_f]\eta = \left(\frac{\partial}{\partial t} + U\frac{\partial}{\partial x}\right)\left(\frac{\partial}{\partial t} + U\frac{\partial}{\partial x}\right)\eta = -\left.\frac{\partial p}{\partial y}\right|_{y=0}. \tag{24}$$

We now recognize that, since the pressure satisfies the Laplace equation, it is possible to interchange its derivatives in x and y in the following way:

$$\frac{\partial}{\partial y} = \pm \mathrm{i}\frac{\partial}{\partial x}. \tag{25}$$

In doing so, one needs to identify which branch is correct. The requirement that perturbations must decay with distance normal to the interface determines that, for downstream-propagating waves, the positive sign be taken on the right-hand side of Eq. (25). We then apply the derivative interchange to the right-hand side of Eq. (24) giving

$$[L_f]\eta = -\mathrm{i}\frac{\partial p_w}{\partial x}. \tag{26}$$

The above could then be integrated in order to find the pressure p_w which drives the wall motion in Eq. (22). Instead, however, we assemble the coupled system model by differentiating Eq. (22) with respect to x and rewriting the right-hand side using Eq. (26). This gives

$$\frac{\partial}{\partial x}([L_w]\eta) = -\mathrm{i}[L_f]\eta. \tag{27}$$

We now proceed to solve Eq. (27). Because there is no variation in wave frequency between regions 1 and 2, we can write

$$\eta(x,t) = \hat{\eta}(x)\exp(-\mathrm{i}\omega t) \tag{28}$$

which, upon substitution into the system equation gives

$$\frac{\mathrm{d}}{\mathrm{d}x}\left(-\omega^2\hat{\eta} + \frac{\mathrm{d}^4\hat{\eta}}{\mathrm{d}x^4} + K(x)\hat{\eta}\right) = -\mathrm{i}\left(-\omega^2\hat{\eta} - 2\mathrm{i}\omega U\frac{\mathrm{d}\hat{\eta}}{\mathrm{d}x} + U^2\frac{\mathrm{d}^2\hat{\eta}}{\mathrm{d}x^2}\right). \tag{29}$$

Eq. (29) is a proper differential equation in x for $\hat{\eta}$ that is amenable to solution using the WKB method. We write

$$\hat{\eta}(x) = \eta_0(x)\exp\left(\mathrm{i}\int k(x)\,\mathrm{d}x\right) = \eta_0 E, \tag{30}$$

where η_0 is a slowly varying function of x. Commensurately, $K(x)$ must be a slowly varying function and we note that its derivative can be written as

$$\frac{\mathrm{d}K}{\mathrm{d}x} = \frac{\mathrm{d}K}{\mathrm{d}k}\frac{\mathrm{d}k}{\mathrm{d}x}. \tag{31}$$

Differentiating out the left-hand side of Eq. (29) gives

$$-\omega^2\frac{\mathrm{d}\hat{\eta}}{\mathrm{d}x} + \frac{\mathrm{d}^5\hat{\eta}}{\mathrm{d}x^5} + K\frac{\mathrm{d}\hat{\eta}}{\mathrm{d}x} + \frac{\mathrm{d}K}{\mathrm{d}k}\frac{\mathrm{d}k}{\mathrm{d}x}\hat{\eta} = -\mathrm{i}\left(-\omega^2\hat{\eta} - 2\mathrm{i}\omega U\frac{\mathrm{d}\hat{\eta}}{\mathrm{d}x} + U^2\frac{\mathrm{d}^2\hat{\eta}}{\mathrm{d}x^2}\right). \tag{32}$$

The solution can now proceed using the substitution of Eq. (30) and retaining terms only up to the first derivative of η_0, using the assumption of slow variation. Upon inspection of Eq. (32) the derivatives required are

$$\frac{\mathrm{d}\hat{\eta}}{\mathrm{d}x} = \left(\mathrm{i}k\eta_0 + \frac{\mathrm{d}\eta_0}{\mathrm{d}x}\right)E, \tag{33a}$$

$$\frac{\mathrm{d}^2\hat{\eta}}{\mathrm{d}x^2} \approx \left(-k^2\eta_0 + \mathrm{i}\frac{\mathrm{d}k}{\mathrm{d}x}\eta_0 + 2\mathrm{i}k\frac{\mathrm{d}\eta_0}{\mathrm{d}x}\right)E, \tag{33b}$$

$$\frac{\mathrm{d}^5\hat{\eta}}{\mathrm{d}x^5} \approx \left(\mathrm{i}k^5\eta_0 + 10k^3\frac{\mathrm{d}k}{\mathrm{d}x}\eta_0 + 5k^4\frac{\mathrm{d}\eta_0}{\mathrm{d}x}\right)E. \tag{33c}$$

After substitution of these into Eq. (32), the $\mathcal{O}(1)$-terms (those terms without explicit x-derivatives) are equated to give

$$-\omega^2 + k^4 + K = \frac{(\omega - Uk)^2}{k}, \tag{34}$$

which, as could be expected, is the dispersion equation, (8), for a wall of uniform flexibility and downstream-propagating waves so that $|k| = k$. Equating the remaining $\mathcal{O}(\mathrm{d}/\mathrm{d}x)$-terms gives

$$\begin{aligned}(-\omega^2 + 5k^4 + K)\frac{\mathrm{d}\eta_0}{\mathrm{d}x} + \left(10k^3 + \frac{\mathrm{d}K}{\mathrm{d}k}\right)\frac{\mathrm{d}k}{\mathrm{d}x}\eta_0 \\ = -2U(\omega - Uk)\frac{\mathrm{d}\eta_0}{\mathrm{d}x} + U^2\frac{\mathrm{d}k}{\mathrm{d}x}\eta_0.\end{aligned} \tag{35}$$

We now multiply Eq. (34) by $\mathrm{d}\eta_0/\mathrm{d}x$ and subtract it from Eq. (35), thereby eliminating K. We also differentiate Eq. (34) with respect to k to obtain an expression for $\mathrm{d}K/\mathrm{d}k$ and then substitute this into Eq. (35) to yield

$$\left[4k^3 + \frac{1}{k^2}(\omega^2 - U^2k^2)\right]\frac{1}{\eta_0}\frac{\mathrm{d}\eta_0}{\mathrm{d}x} + \left[6k^2 - \frac{1}{k^3}\omega^2\right]\frac{\mathrm{d}k}{\mathrm{d}x} = 0. \tag{36}$$

Inspection of Eq. (36) shows that it can be rewritten as

$$\frac{\mathrm{d}}{\mathrm{d}x}\{\eta_0^2[4k^3 + (\omega^2 - U^2k^2)/k^2]\} = 0,$$

and, finally, integration between $x = x_1$ (where $k = k_1$, $\eta_0(x_1) = \eta_{01}$) and x_2 (where $k = k_2$, $\eta_0(x_2) = \eta_{02}$) gives the amplitude-ratio result

$$A_{21} = \frac{\eta_{02}}{\eta_{01}} = \left[\frac{4k_1^3 + (\omega^2 - U^2k_1^2)/k_1^2}{4k_2^3 + (\omega^2 - U^2k_2^2)/k_2^2}\right]^{1/2}, \tag{37}$$

which is the same as the result of Eq. (21a), derived using the system energy equation, for the case of waves with positive wavenumber. For upstream-propagating waves, the analysis is repeated using the negative sign in Eq. (25). The result of this exercise can be combined with that of Eq. (37) to give Eq. (21a) that equally well holds for both upstream- and downstream-propagating waves.

We now briefly assess the magnitude of terms omitted in generating the approximate expressions of Eqs. (33b) and (33c). We recall that higher-order, and products of first-order, derivatives of k and η_0 with respect to x were neglected. The physical system studied has slow variation of the foundation spring stiffness; hence we introduce a small parameter, ε, such that $\mathrm{d}K/\mathrm{d}x \approx (K_2 - K_1)/(x_2 - x_1) = \mathcal{O}(\varepsilon)$. From Eq. (31), it is then evident that $\mathrm{d}k/\mathrm{d}x = \mathcal{O}(\varepsilon)$ provided that $\mathrm{d}K/\mathrm{d}k = \mathcal{O}(1)$. This condition is seen to be satisfied by differentiating the dispersion relation, Eq. (34), with respect to k. We now consider the magnitude of $\mathrm{d}\eta_0/\mathrm{d}x$. Using primes as shorthand for differentiation of K with respect to k, we note from inspection that Eq. (36) can alternatively be written as

$$\frac{2}{\eta_0}\frac{\mathrm{d}\eta_0}{\mathrm{d}x} + \frac{K''}{K'}\frac{\mathrm{d}k}{\mathrm{d}x} = 0. \tag{38}$$

Because K', K'' and successive derivatives are all $\mathcal{O}(1)$, and, as shown above, $\mathrm{d}k/\mathrm{d}x = \mathcal{O}(\varepsilon)$, it is clear that $\mathrm{d}\eta_0/\mathrm{d}x = \mathcal{O}(\varepsilon)$. It is also straightforward to show that $\mathrm{d}^n(\eta_0, k)/\mathrm{d}x^n$ is of the same order as $\mathrm{d}^nK/\mathrm{d}x^n = \mathcal{O}(\varepsilon^n)$ where $\varepsilon = \mathcal{O}(1/(x_2 - x_1))$; the data that produced the results in Figs. 5–9 has $1/(x_2 - x_1) \approx 0.005$. Our analysis, therefore, has omitted $\mathcal{O}(\varepsilon^2)$ and higher terms in generating the approximate amplitude-ratio result of Eq. (37).

In closing this section, we note that the amplitude-ratio formulae for line-excitation on a homogeneous flexible wall and wave propagation on a spatially inhomogeneous flexible wall are closely related. Defining a function

$$f(k, \omega, U) = 4k^3 + (\omega^2 - U^2k^2)/(|k|k), \tag{39}$$

the amplitude ratio for waves propagating downstream and upstream from a point of line excitation, Eq. (12a), can be written as

$$A_{DU} = \left|\frac{f(k_U, \omega, U)}{f(k_D, \omega, U)}\right|, \tag{40}$$

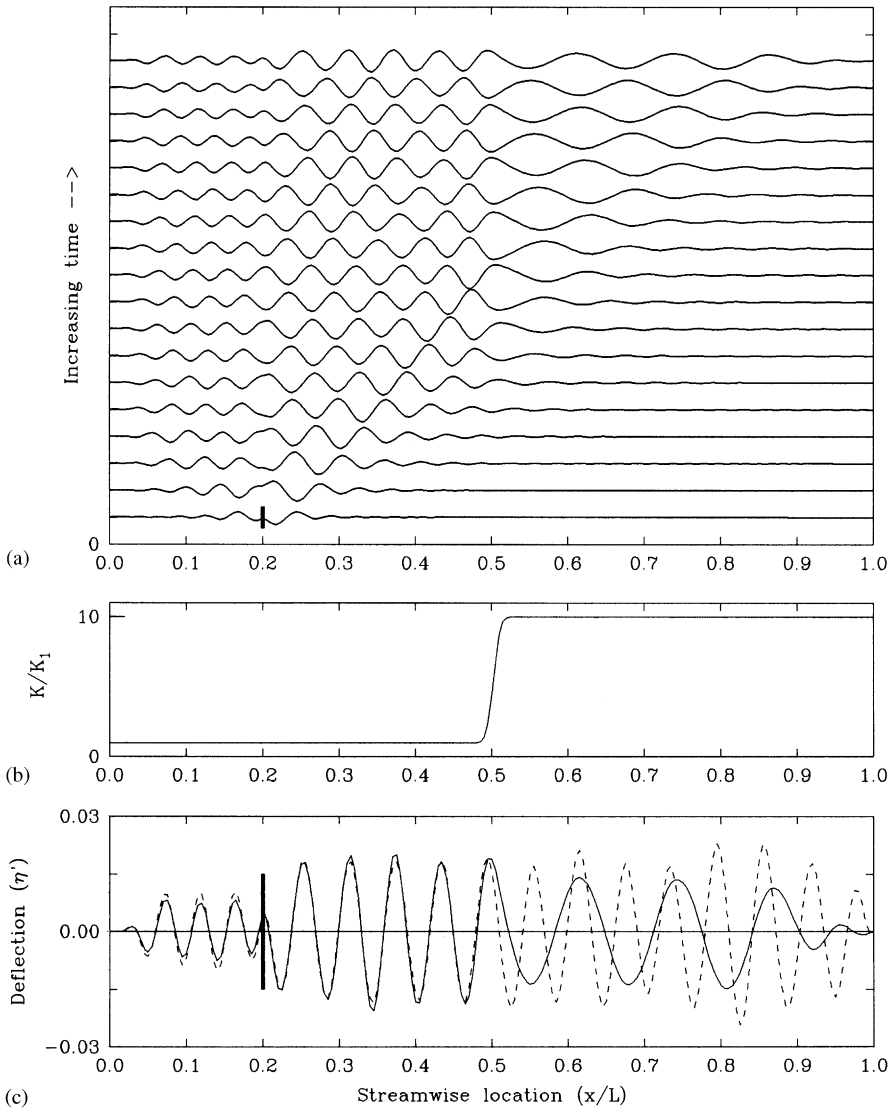

Fig. 9. Propagation of waves from applied oscillatory excitation on a spatially inhomogeneous flexible wall with a rapid change in properties: (a) wall profiles in space–time form, (b) Variation of spring-stiffness coefficient along wall, and (c) comparison of waves for a homogeneous, $K/K_1 = 1$, wall (– – –) and those on the spatially varying flexible wall (——). All data are identical to those of Fig. 5 except that here $\sigma = 0.01$.

where ω $(= \omega_F)$ is the frequency of both the upstream and downstream waves. Similarly, the amplitude ratio for incoming and outgoing waves on either side of region of change in flexible-wall properties, Eq. (21a), can be re-written as

$$A_{21} = \sqrt{\frac{f(k_1, \omega, U)}{f(k_2, \omega, U)}}. \tag{41}$$

4.3. Rapid change in flexible-wall properties

The analyses developed in Sections 4.1 and 4.2 above are based upon the premise of single-wave disturbances, propagating in the same direction, in each of regions 1 and 2. This premise is found to be valid for a slow change in

flexible-wall properties, as borne out by the agreement between the results of simulations and theory seen in Fig. 5. In the WKB approach, the assumption of slow change is actually implicit. We now briefly consider the case of wave-propagation through a region of rapid change. Fig. 9 therefore summarizes a numerical experiment in which all the data are exactly the same as in Fig. 5 except that $K(x)$ is now evaluated using $\sigma = 0.01$ in Eq. (13). This gives a very rapid change in wall properties as can be seen in Fig. 9b. Contrasting the results in Fig. 9 with those in Fig. 5, the key difference is that an element of wave reflection now occurs from the region of change in flexible-wall properties. This is most clearly seen in Fig. 9c where, upstream of the region of change, there is no longer exact equivalence between the wave response of a homogeneous flexible wall and that of the spatially varying flexible wall. Detailed inspection shows that the wave in the region x: $0.2 \rightarrow 0.45$ comprises the usual (k_1, ω)-wave and a low-intensity contribution from an upstream-propagating, (k_U, ω)-wave, of the exactly the same type that exists upstream of the driver in the region x: $0 \rightarrow 0.2$. This latter component is launched by the partial reflection of the (k_1, ω)-wave incident on the region of rapid change. As it passes through $x = 0.2$, it enters the region upstream of the line excitation and combines with a wave of exactly the same characteristics that originates directly from the line excitation. The 'reflected wave' has undergone a phase reversal and its contribution therefore reduces the amplitude of the wave response in this region.

The results in Fig. 9 serve to highlight the limitations of the theory developed in Sections 4.1 and 4.2. Other numerical experiments show that the wave-reflection phenomenon is entirely absent for the range of $\sigma = 0.15$ down to $\sigma = 0.05$. Given the very low intensity of the reflected wave-energy in Fig. 6, it seems that $\sigma = 0.01$ represents an approximate threshold for a tenfold change in K. Clearly, further theoretical developments will need to incorporate the upstream propagating wave that is launched by the incidence of the downstream-propagating wave on the region of rapid change in flexible-wall properties.

5. Conclusion

Numerical simulation and theoretical analysis have been combined in a complementary approach to study the excitation of neutrally stable waves on a plate-spring type of flexible wall. A formula has been derived to relate the amplitude of waves downstream of a point of applied oscillatory excitation to those waves that propagate upstream of it. The phenomenon of amplitude difference between such waves is found to be attributable to the selective distribution of energy that originates from the line excitation.

The evolution of neutrally stable waves, as they travel from one region of a flexible wall to another with different properties, has been studied. With slowly changing wall properties prescribed, it is found that each of the waves on either side of the region of change is accurately described by the dispersion equation based on local wall properties. An amplitude-ratio formula linking the incoming and outgoing waves has been derived through two independent methods. In the first, wave energy fluxes of the fluid-structure system are balanced on either side of the region of change. The second, WKB method, performs the analysis at the level of system forces. The WKB method is anticipated to be useful in the study of more refined flexible-wall and fluid models because it can be adapted to incorporate nonconservative system energy exchanges in the region of changing wall properties.

The effects of a rapid change in wall properties have been briefly considered. Numerical simulations show that, for example, a downstream propagating wave incident upon a region of rapidly increasing wall stiffness yields both a transmitted wave and generates a 'reflected' upstream propagating wave that, like the incident and transmitted waves, is a solution of the dispersion equation based on local wall properties. More advanced theoretical treatments will need to address the phenomenon of energy scattering by a rapid change in flexible-wall properties.

Finally, we remark that the present work requires extension to study the effect of changing wall properties on unstable waves. It is anticipated that a flexible wall with spatial variation in its properties could be used to limit the growth of hydroelastic instability. What has been achieved in the present paper is the establishment of a framework for the study of fluid-structure interactions in spatially varying systems.

Acknowledgement

The authors gratefully wish to acknowledge the support of the UK Engineering and Physical Sciences Research Council through the award of a Visiting Research Fellowships that enabled Professor P.K. Sen to visit the University of Warwick during which time much of the work reported above was carried out.

References

Abrahams, I.D., Wickham, G.R., 2001. On transient oscillations of plates in moving fluids. Wave Motion 33, 7–23.

Brazier-Smith, P.R., Scott, J.F., 1984. Stability of fluid flow in the presence of a compliant surface. Wave Motion 6, 547–560.

Carpenter, P.W., Garrad, A.D., 1986. The hydrodynamic stability of flow over Kramer-type compliant surfaces. Part 2. Flow-induced surface instabilities. Journal of Fluid Mechanics 170, 199–232.

Carpenter, P.W., Davies, C., Lucey, A.D., 2000. Hydrodynamics and compliant walls: does the dolphin have a secret? Current Science 79, 758–765.

Carpenter, P.W., Lucey, A.D., Davies, C., 2001. Progress on the use of compliant walls for laminar-flow control. AIAA: Journal of Aircraft 38, 504–512.

Choi, K.-S., Yang, X., Clayton, B.R., Glover, E.J., Altar, M., Semenov, B.N., Kulik, V.M., 1997. Turbulent drag reduction using compliant surfaces. Proceedings of the Royal Society of London A 453, 2229–2240.

Crighton, D.G., Oswell, J.E., 1991. Fluid loading with mean flow. I. Response of an elastic plate to localized excitation. Philosophical Transactions of the Royal Society of London A 335, 557–592.

Davies, C., Carpenter, P.W., 1997. Numerical simulation of the evolution of Tollmien-Schlichting waves over finite compliant panels. Journal of Fluid Mechanics 335, 361–392.

De Langre, E., Ouvrard, A.E., 1999. Absolute and convective bending instabilities in fluid-conveying pipes. Journal of Fluids and Structures 13, 663–680.

Lucey, A.D., 1998. The excitation of waves on a flexible panel in a uniform flow. Philosophical Transactions of the Royal Society of London A 356, 2999–3039.

Lucey, A.D., Carpenter, P.W., 1992. A numerical simulation of the interaction of a compliant wall and an inviscid flow. Journal of Fluid Mechanics 234, 121–146.

Lucey, A.D., Peake, N., 2003. Wave excitation on flexible walls in the presence of a fluid flow. In: Carpenter, P.W., Pedley, T.J. (Eds.), IUTAM: Flow through collapsible tubes and past other highly compliant boundaries. Kluwer Academic Publishers, The Netherlands, pp. 118–145 (Chapter 6).

Peake, N., 1997. On the behaviour of a fluid-loaded cylindrical shell with mean flow. Journal of Fluid Mechanics 338, 387–410.